A Data-Adaptive Ocean Wave Directional-Spectrum Estimator for Pitch and Roll Type Measurements

JOAN OLTMAN-SHAY AND R. T. GUZA

Center for Coastal Studies, Scripps Institution of Oceanography, La Jolla, CA 92093

(Manuscript received 1 June 1984, in final form 13 August 1984)

ABSTRACT

A data-adaptive directional-spectrum estimator is developed for "point" measurement systems such as the pitch and roll buoy and slope array. This estimator, unlike the much employed unimodal cosine power parameterization method of Longuet-Higgins and others, does not make *a priori* assumptions about the shape of the directional spectrum. Instead improved resolution is obtained with a maximum likelihood method similar to those successfully used with spatial arrays. The numerical algorithm is relatively simple and computationally fast. The capabilities and limitations of the new estimator are illustrated with a variety of synthetic directional spectra. The estimator is applied to field data obtained from a slope array in 9 m depth at Santa Barbara, California and is found to yield physically realistic directional spectra. It marginally resolves two directional modes that topographical features dictate should be separated by approximately 70 degrees.

1. Introduction

Wind-generated surface gravity waves are a principle source of energy to oceanic coastlines. A complete description of the incident wave field requires well resolved estimates of both frequency and directional spectra. Significant progress has been made in the design of spatial wave arrays and in the refinement of the associated analysis techniques (Davis and Regier, 1977; Long and Hasselmann, 1979; Pawka, 1982, 1983; Pawka *et al.*, 1983, 1984). Although spatial arrays yield high resolution directional spectra, they are difficult to install and maintain. They require spatial homogeneity over their entire length (several hundred meters for high resolution of long swell) which is a condition not generally met in shallow water. Bottom-mounted arrays in deeper water suffer from attenuation of the wave signals, as well as a host of logistics problems. The difficulty associated with deploying long linear arrays in any depth of water is reflected in the relatively few times they have been implemented.

Compact "point" measurement systems such as the pitch-and-roll buoy (Longuet-Higgins *et al.*, 1963) have successfully yielded directional wave data in the field. Point systems comprised of fixed instruments, such as the pressure sensor–current meter combination (Nagata, 1964; Bowden and White, 1966) and "slope array" (Seymour and Higgins, 1977; Higgins *et al.*, 1981), have also been widely used to sample wave directional statistics. The pitch-and-roll buoy, slope array, and pressure–current measurement systems have formally equivalent directional resolution.

Point measurement systems with theoretically higher resolution have been deployed, but have not yielded definitive results. For example, the theoretical response of the "cloverleaf buoy" to a directional spike in the true spectrum has roughly half the bandwidth of the pitch-and-roll buoy (Cartwright and Smith, 1964). However, lacking a standard for comparison, Cartwright and Smith find their cloverleaf results only to be "reasonable". One of the most widely cited cloverleaf buoy papers, that by Mitsuyasu *et al.* (1975), actually uses pitch-and-roll-type data (contained as a subset of the cloverleaf data) for most of the wave analysis. The added information of the cloverleaf system was judged to "contain non-negligible errors, due to the poor accuracy in the measurement of wave curvature." The theoretically higher resolution of the cloverleaf buoy has not been convincingly shown to be realizable in field applications. Simpson (1969) showed that an array of three fixed biaxial current meters has resolving power equivalent to the cloverleaf buoy. In a field application, the current meter array was judged to be "only partially successful." Borgman and Yfantis (1979) concluded that their tower-mounted 8-element (4 on a single vertical level) flowmeter array, although theoretically capable of yielding higher resolution spectra, only reliably produced resolution slightly better than a pitch-and-roll buoy. The signal-to-noise ratio apparently became small when using closely spaced sensors to calculate high-order derivatives of the flow field.

Motivated by the need for improved resolution, and the limited success in improving the basic point measurement system, attention is given here to im-

© 1984 American Meteorological Society

proving the resolution of the directional estimates which can be obtained from the ubiquitous pitch-and-roll buoy (and the theoretically equivalent slope array and pressure-current systems). Two of the three standard analysis methods for point measurement systems (Longuet-Higgins, *et al.*, 1963) produce very low resolution estimates; their response to a spike in the true directional spectrum is highly smeared, with a Full Width at Half Maximum power (FWHM) of 88 and 131 degrees. These two methods estimate the spectrum with a truncated Fourier series whose coefficients are obtained from the cross-spectral data matrix [Eq. (1)] acquired with pitch-and-roll-buoy (and equivalent) systems. One of these methods weights the coefficients to avoid negative-valued spectra.

Longuet-Higgins *et al.* (1963) fully appreciated the fact that these estimators give large overestimates of the width of a relatively narrow true directional spectra. In order to obtain more realistic spectral characteristics, they proposed schemes based on *a priori* assumptions about the shape of the directional spectrum. Various combinations and ratios of the elements of the cross-spectral data matrix (Eq. 1) were compared with the values that would result if the true directional spectrum were one of 3 unimodal forms (cosine power, quasi-normal, square-topped gate). Although there was considerable scatter, their limited data set was most consistent with the form

$$\hat{E}(f, \theta) = K\left[\cos\left(\frac{\theta - \alpha}{2}\right)\right]^{2S},$$

where K, α, S are free parameters and functions of frequency.

These three free parameters can be determined using only 3 elements in the 6-element cross-spectral matrix. The additional elements can be used as a check on the internal consistency of the assumed distribution. Cartwright (1963) observed inconsistencies in the assumed cosine power distribution using this check and remarked on the likelihood of bimodal spectra. He still used the unimodal cosine power form because consideration of bimodality (and presumably non-cosine unimodal forms) was "considered too complicated to try to take into account . . . for this work." In other cases when the check reveals an inconsistency with the assumed directional form, there seems to be a tendency to question the accuracy of the higher-order matrix elements rather than the assumed directional form (Mitsuyasu *et al.*, 1975; Forristall *et al.*, 1978). This decision seems arbitrary.

Borgman and Yfantis (1979) suggested that storm waves can be assumed to be directionally unimodal and that the cosine parameterization applied to pitch-and-roll buoy (or equivalent) data can provide enough information for most purposes. Their suggestion was founded on measurements taken during several local storms using their 8-element flowmeter array that produced spectra with only slightly better resolution than a pitch-and-roll buoy. We note, however, that several investigations have suggested the occurrence of directional bimodality (within a frequency band) caused by different wind systems (Cartwright, 1963; Longuet-Higgins *et al.*, 1963; Simpson, 1969) or coastal topographic effects (Pawka, 1983; Pawka *et al.*, 1984). Differences in these observations from those of Borgman and Yfantis may result from the fact that the latter took measurements under locally high winds so that wave energy propagating from distant areas may have been relatively unimportant compared to locally generated waves.

Regier and Davis (1977) deployed a relatively high-resolution spatial array from the Research Platform FLIP, stationed in the open ocean about 300 km east of Barbados. They estimated ocean directional spectra daily for a one month period and concluded that the wave spectrum under typical rather than carefully chosen oceanic conditions is not solely determined by local winds, but is the result of the temporal and spatial history of winds experienced by the waves. The directional spectra they observed had a wide variety of shapes and were convincingly demonstrated to be inconsistent with a cosine power distribution. This raised "serious questions with regard to the practices of fitting observations to simple models derived from prescribed directional spectra."

The assumption of a unimodal cosine power distribution in cases other than strong local winds appears to be unjustified and therefore limits the usefulness of the cosine parameter-fit method. The two alternative truncated Fourier series methods, although without *a priori* power distribution assumptions, have very poor resolution. Long and Hasslemann (1979) have developed a directional spectrum estimator for spatial arrays that they point out is adaptable to point measurement systems. Nonetheless, the three methods of Longuet-Higgins *et al.* (1963) are still the most widely used directional estimators for point measurement systems. In Section 2, a new data-adaptive estimator is derived that does not require assumptions about the directional power distribution form. In Section 3, the new algorithm (a maximum likelihood estimator) is tested with a variety of synthetic directional spectra and its capabilities and limitations are discussed. In Section 4, the new estimator is applied to field data obtained with a bottom-mounted pressure sensor slope array in 9 m of water at Santa Barbara, California. It is found to yield physically realistic directional spectra.

2. Theory

An ideal slope array (Seymour and Higgins, 1977) or pitch-and-roll buoy (Longuet-Higgins, *et al.*, 1963) provides time series of the variables η, η_x and η_y where $\eta(x, y, t)$ is the sea surface elevation, x, y are horizontal coordinates, and a subscripted independent

variable indicates differentiation with respect to that variable. With C and Q the co-spectrum and the quadrature spectrum between any two measured variables, it is readily shown (Longuet-Higgins *et al.*, 1963) that

$$\left.\begin{aligned}
C_{11}(f) &= C[\eta(f)\eta(f)] = \int_0^{2\pi} E(f,\theta)d\theta \\
Q_{12}(f) &= -Q[\eta(f)\eta_x(f)]k^{-1} \\
&= -\int_0^{2\pi} E(f,\theta)\cos\theta d\theta \\
Q_{13}(f) &= -Q[\eta(f)\eta_y(f)]k^{-1} \\
&= -\int_0^{2\pi} E(f,\theta)\sin\theta d\theta \\
C_{22}(f) &= C[\eta_x(f)\eta_x(f)]k^{-2} \\
&= \int_0^{2\pi} E(f,\theta)\cos^2\theta d\theta \\
C_{23}(f) &= C[\eta_x(f)\eta_y(f)]k^{-2} \\
&= \int_0^{2\pi} E(f,\theta)\sin\theta\cos\theta d\theta \\
C_{33}(f) &= C[\eta_y(f)\eta_y(f)]k^{-2} \\
&= \int_0^{2\pi} E(f,\theta)\sin^2\theta d\theta
\end{aligned}\right\}, \quad (1)$$

where $E(f, \theta)$ is the energy density at frequency f, angle θ, and k is the scalar wavenumber (given by linear theory). The C_{nm} and Q_{nm} are the elements of the normalized (by factors of k) cross-spectral data matrix, $\mathbf{M}_{nm}$, where

$$\mathbf{M}_{nm} = C_{nm} + iQ_{nm}, \quad C_{mn} = C_{nm}^* \text{ for } n \neq m.$$

The new spectrum estimator, like the three estimators of Longuet-Higgins *et al.* (1963), operates on this cross-spectral data matrix. It does not make *a priori* assumptions about the shape of the directional spectrum. It achieves improved resolution with *a posteriori* assumptions about the directional spectrum; assumptions that are founded on the input data. This class of *a posteriori* estimators is often referred to as data adaptive. The new data-adaptive estimator developed here is closely related to the maximum likelihood estimator (MLE) developed for spatial arrays by Capon *et al.* (1967). The following derivation directly parallels Davis and Regier's (1977) discussion of the MLE for spatial arrays.

Capon *et al.* (1967) originally presented their method as an estimator of the most likely complex amplitude $A(\alpha, f)$ of a single plane wave in noise which has a joint Gaussian probability distribution. For a point array system, an MLE amplitude estimate is a linear combination of the Fourier coefficients of η, η_x and η_y (denoted by F_1, F_2, F_3, respectively) so that

$$\hat{A}(\alpha, f) = \sum_{n=1}^{3} w_n(\alpha, f)F_n(f), \quad (2)$$

where w_n are complex weighting functions. A variance estimate would then be

$$\begin{aligned}
\hat{E}(\alpha) = \hat{A}(\alpha)\hat{A}^*(\alpha) &= \sum_{n=1}^{3}\sum_{m=1}^{3} w_n(\alpha)w_m^*(\alpha)F_nF_m^* \\
&= \sum_{n=1}^{3}\sum_{m=1}^{3} w_n(\alpha)w_m^*(\alpha)\mathbf{M}_{nm}, \quad (3)
\end{aligned}$$

where $\mathbf{M}_{nm}$ is the complex cross-spectral data matrix of Eq. (1) and has the form,

$$\mathbf{M}_{nm} = \int_0^{2\pi} E(\theta)G_n(\theta)G_m^*(\theta)d\theta,$$

where $G_1 = 1$, $G_2 = i\cos\theta$ and $G_3 = i\sin\theta$. The frequency notation has been dropped. If the wave field consists of a single plane wave of variance $E(\alpha)$ embedded in noise, the spectrum has the form,

$$E(\theta) = \delta(\theta - \alpha)E(\alpha) + E_N(\theta),$$

where $E_N(\theta)$ is the noise spectrum. The variance estimate at angle α is then

$$\begin{aligned}
\hat{E}(\alpha) &= \sum_{n=1}^{3}\sum_{m=1}^{3} w_n(\alpha)w_m^*(\alpha)\mathbf{M}_{nm} \\
&= E(\alpha)W(\alpha,\alpha) + \int_0^{2\pi} W(\alpha,\theta)E_N(\theta)d\theta, \quad (4)
\end{aligned}$$

where $W(\alpha, \theta)$ is a window function of the form,

$$W(\alpha,\theta) = \sum_{n=1}^{3}\sum_{m=1}^{3} w_n(\alpha)w_m^*(\alpha)G_n(\theta)G_m^*(\theta).$$

Substituting in the values of $G_n(\theta)$,

$$W(\alpha,\theta) = |w_1(\alpha) + iw_2(\alpha)\cos\theta + iw_3(\alpha)\sin\theta|^2.$$

As Davis and Regier (1977) point out, this variance estimate (Eq. 4) is a maximum likelihood estimate if a constraint of unity gain of the signal $E(\alpha)$ in the absence of noise is imposed so that

$$\begin{aligned}
W(\alpha,\alpha) = |w_1(\alpha) + iw_2(\alpha)\cos\alpha \\
+ iw_2(\alpha)\sin\alpha| = 1, \quad (5a)
\end{aligned}$$

$$\hat{E}(\alpha) = E(\alpha) + \int_0^{2\pi} W(\alpha,\theta)E_N(\theta)d\theta. \quad (5b)$$

Minimizing the convolution of $W(\alpha, \theta)$ and $E_N(\theta)$ in Eq. (5b) minimizes the error in the $\hat{E}(\alpha)$ estimate. Since $E(\alpha)$, $W(\alpha, \theta)$ and $E_N(\theta)$ are all nonnegative, minimizing the convolution is equivalent to minimizing $\hat{E}(\alpha)$ of Eq. (3) itself. Subjecting the minimi-

zation to the constraint [Eq. (5a)] leads to the final form of the estimator,

$$\hat{E}(\alpha) = \{\sum_{n=1}^{3}\sum_{m=1}^{3} \mathbf{M}_{nm}^{-1} G_n(\alpha) G_m^*(\alpha)\}^{-1}, \quad (6)$$

where $\mathbf{M}_{nm}^{-1}$ is the inverse of $\mathbf{M}_{nm}$. This new point-measurement maximum likelihood estimator of spectra will be referred to as the MLE. An attractive feature of the MLE is its computational speed and simplicity. The algorithm requires only one inversion of the 3×3 complex $\mathbf{M}_{nm}$ per frequency bin.

Another spectrum estimator we will present here is intimately related to the MLE and achieves higher resolution. It is the iterative maximum likelihood estimate (IMLE) developed by Pawka (1982, 1983) for spatial arrays. The application to point measurement systems is straightforward.

The IMLE algorithm is founded on a recognition of the smoothing nature of the MLE, demonstrated by Burg (1972) in his quantitative analysis of the relationship between the maximum entropy method (MEM) and the MLE. The MEM yields a possible true spectrum because the spectrum can be used to retrieve the original cross-spectral matrix. However, the MLE spectrum is not consistent with the original matrix elements. Burg showed the MLE spectrum is an average of the MEM spectra obtained from its N-point estimation scheme; the 1-point estimate having the lowest resolution. The MLE spectrum is an average of low- and high-resolution MEM spectra and therefore is a smoothed N-point MEM spectrum. The MLE has nonetheless played an active role in wave directional analysis (Regier and Davis, 1977; Davis and Regier, 1977; Pawka, 1982, 1983) because it can be applied to unequal-lag spatial arrays. The MEM requires equal-lag spatial arrays.

The IMLE spectrum, like the MEM spectrum, is a possible true spectrum. The iterative algorithm develops a spectrum that can be used to reconstruct the original cross-spectral matrix. The original MLE spectrum is iteratively modified in the IMLE algorithm to move closer to a possible true spectrum by examining the behavior of MLE. In notational terms, the IMLE algorithm is

$$\hat{E}_{\mathrm{IMLE}}^{i}(\alpha) = \hat{E}_{\mathrm{IMLE}}^{i-1}(\alpha) + \epsilon_i(\alpha), \quad (7)$$

where $\epsilon_i(\alpha)$ is the modification to the $i-1$ iteration. Pawka (1982, 1983) defines $\epsilon_i(\alpha)$ as

$$\epsilon_i(\alpha) = \frac{|\lambda|^{\beta+1}}{\lambda} \frac{\hat{E}_{\mathrm{IMLE}}^{i-1}(\alpha)}{\gamma}, \quad (8a)$$

$$\lambda = 1.0 - \frac{T_{\mathrm{MLE}}^{i-1}(\alpha)}{\hat{E}_{\mathrm{IMLE}}^{0}(\alpha)}, \quad (8b)$$

where $T_{\mathrm{MLE}}^{i-1}(\alpha)$ is a MLE spectrum estimate from a cross-spectral matrix reconstructed from $\hat{E}_{\mathrm{IMLE}}^{i-1}$, $\hat{E}_{\mathrm{IMLE}}^{0}$ the original MLE spectrum estimate and β and γ are variable parameters that dictate the convergence rates of the IMLE algorithm. Here $T_{\mathrm{MLE}}^{i-1}(\alpha)$ approaches $\hat{E}_{\mathrm{IMLE}}^{0}(\alpha)$ with increasing iterations and the iterative cross-spectral matrix elements should approach the original matrix element values. The latter convergence is not an explicit constraint of the iterative scheme, but appears to be a natural consequence of it. The cross-spectral matrix elements were monitored throughout synthetic and field data analysis and were always found to converge to the original matrix element values.

Another iterative correction term examined here did not have the peak/trough asymmetry of the Pawka $\epsilon_i(\alpha)$ term [Eq. (8)]. Using Eq. 8, iterative corrections are larger for the energetic regions of the spectrum. In addition, the form of Eq. (8b) develops an asymmetry in the positive and negative values of λ resulting in a bias towards negative corrections. An alternative symmetric correction term (IMLEO) is as follows,

$$\epsilon_i(\alpha) = \frac{|\lambda|^{\beta+1}}{\gamma\lambda}, \quad (9a)$$

$$\lambda = \hat{E}_{\mathrm{IMLE}}^{0}(\alpha) - T_{\mathrm{MLE}}^{i-1}(\alpha). \quad (9b)$$

Synthetic and field data have demonstrated an insensitivity to these two forms of iterative correction terms. The energetic regions of the spectra are virtually indistinguishable. Not unexpectedly, synthetic data testing does allude to a strong dependence of the IMLE spectrum on the original MLE spectrum. If the MLE spectrum is a reasonable estimate of the true spectrum, as it appears to be in many cases, the IMLE will be as good an estimate or better. A conservatively slow convergence was chosen ($\beta = 1.0$, $\gamma = 20$) with 50 iterations for both synthetic and field data.

3. Synthetic data tests

The objective of this section is to test the capabilities of the three data-adaptive estimators, MLE, IMLEP, and IMLEO (Eqs. 6, 8, 9). The truncated Fourier series estimators will be briefly mentioned here only to provide an evaluation of their performance relative to that of the data-adaptive estimators. Their performance, measured by a variety of criteria mentioned below, was always significantly inferior to that of the three data adaptive estimators.

The test data can be divided into two major categories, deterministic and nondeterministic. Both use cross-spectral matrices generated from test spectra of the form

$$E(\alpha) = E_p(\alpha) + E_N(\alpha),$$

where $E_N(\alpha)$ is the uniform background noise and

$$E_p(\alpha) = \sum_{n=1}^{n_p} P_n \exp[-(\alpha - \alpha_n)^2/(2\sigma_n^2)]. \quad (10)$$

In (10) $E_p(\alpha)$ has n_p peaks, each peak having a

maximum value of P_n at angle α_n. Test spectra using a cosine power instead of a Gaussian distribution were also used with no significant change in estimator performance. Nondeterministic matrices were generated by assuming Gaussian-distributed Fourier coefficients and are discussed later.

The performance of spectrum estimators that operate upon cross-spectral matrices generated from point-measurement systems is independent of frequency and wavenumber. Unlike cross-spectral matrices from spatial arrays, point-measurement matrices do not contain any frequency or wavenumber information that cannot be normalized out [Eq. (1)]. However, the quality of these measured cross-spectral elements is dependent upon sensor accuracy, wavenumber and other factors. For example, the optimal spacing between slope array elements is a function of wavenumber (Higgins *et al.*, 1981). For a given slope array geometry, slopes will be accurately measured only within some wavenumber range. Such measurement problems are not considered here. The spectrum estimators are also not affected by the directional location of the peak mode angle. However, the estimator's ability to resolve two or more modes is dependent on the angular separation of the modes.

We have used deterministic spectra to address the performance of the spectrum estimators with varying uniform background noise levels and a variety of directional mode widths and angular separations of modes. Two fidelity measures are defined to quantify the degree of agreement between true, $E(\alpha)$ and estimated, $\hat{E}(\alpha)$ spectra. The average percent error (APE)

$$\text{APE} = \frac{1}{n_\alpha} \sum_\alpha \left(\frac{|\hat{E}(\alpha) - E(\alpha)|}{E(\alpha)} \right) \times 100, \qquad (11)$$

where n_α is the number of directional bins, is an overall index of the estimator fidelity. High- and low-energy regions equally influence the value of APE. An alternative index, the weighted average percent error (WAPE)

$$\text{WAPE} = \frac{\sum_\alpha |\hat{E}(\alpha) - E(\alpha)|}{\sum_\alpha E(\alpha)} \times 100 \qquad (12)$$

weights the energetic region of the spectrum over low-energy regions. Large percentage errors in the low-energy regions do not necessarily lead to large values of WAPE.

The effect of uniform background noise levels was examined for unimodal and bimodal spectra. The amount of background noise, relative to the deterministic signal [the noise-to-signal ratio (NSR)]

$$\text{NSR} = \frac{\sum_\alpha E_N(\alpha)}{\sum_\alpha E_p(\alpha)} \qquad (13)$$

varied from 0.001 to 0.2. Figure 1 shows the WAPE fidelity of the estimators for a bimodal spectrum as a function of NSR. The modes have 10 degrees full width at half maximum power (FWHM) and are separated by 90 degrees. A monotonic performance degradation of all three estimators with increased noise is shown. However, a monotonic degradation was not always observed. Unimodal spectra with low NSR values would sometimes be over-resolved by both of the IMLE algorithms and thereby slightly decrease WAPE performance relative to higher NSR values. In general, unimodal test spectra show a dependence on the NSR similar to bimodal spectra. In all cases the IMLEP and IMLEO outperformed the MLE. Figure 2 shows a bimodal test spectrum used in Fig. 1 (NSR = 0.05) and its associated estimated spectra. Even for a WAPE value in excess of 100 (the MLE spectrum), the general shape of the estimated spectrum is reproduced reasonably well.

The FWHM of a unimodal test spectrum (NSR = 0.05) was varied from 3 to 45 degrees. Figures 3 and 4 show the true FWHM and full width at average power (FWAP) respectively against the estimated values. The average power is the power level if the frequency band energy was isotropically distributed. Both IMLE methods underestimate the true FWHM of the mode whereas the MLE is in very good

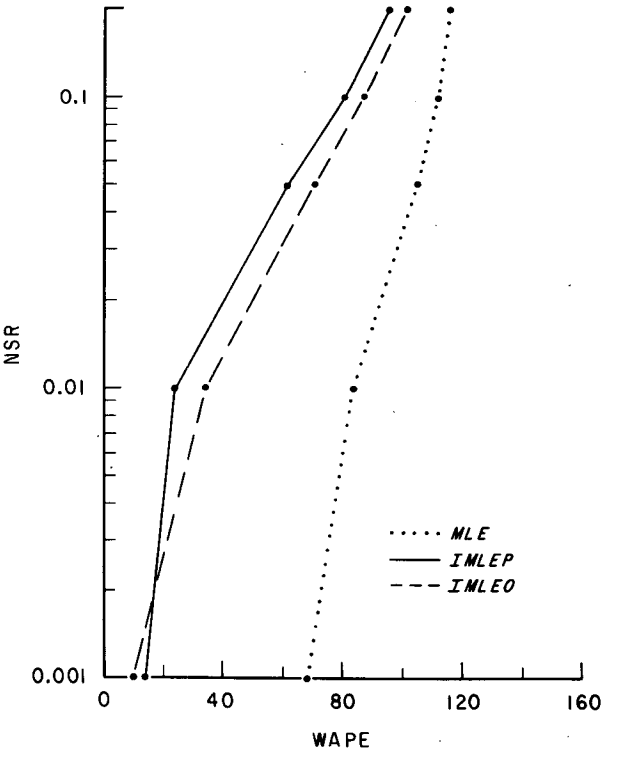

FIG. 1. The weighted average percent error (WAPE) fidelity of a bimodal spectrum with varying noise-to-signal ratio (NSR). The two directional modes are of equal energy with 10 degrees full width at half-maximum power and are separated by 90 degrees.

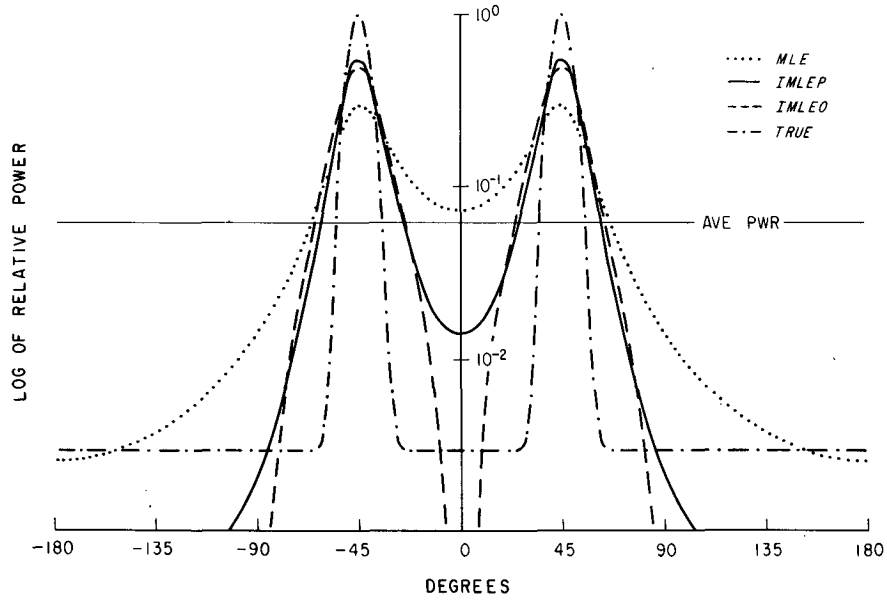

FIG. 2. A true bimodal directional spectrum (NSR = 0.05) and the MLE, IMLEP and IMLEO estimated spectra. The true spectrum modes are 10 degrees full width at half maximum power.

agreement (Fig. 3). However, the IMLE methods outperform the MLE in estimating FWAP (Fig. 4). For these test spectra, the average power level is lower than the mode's half-power level so that the above observations reflect the tendency of the IMLE to underestimate the width of the upper portion of the mode. An example of estimator performance for a true unimodal spectrum with a 10-degree FWHM is given in Fig. 5.

Although the MLE outperforms the IMLE in estimating certain mode-width parameters, the IMLE has superior overall performance. In all the unimodal test spectra of Figs. 3 and 4, the weighted average percent error (WAPE) values are smaller for the IMLE than for the MLE (Fig. 6). In addition, the average error in the estimated percent power in the mode was 7.8% for the MLE whereas it was 0.69% and 1.1% for the IMLEP and IMLEO respectively.

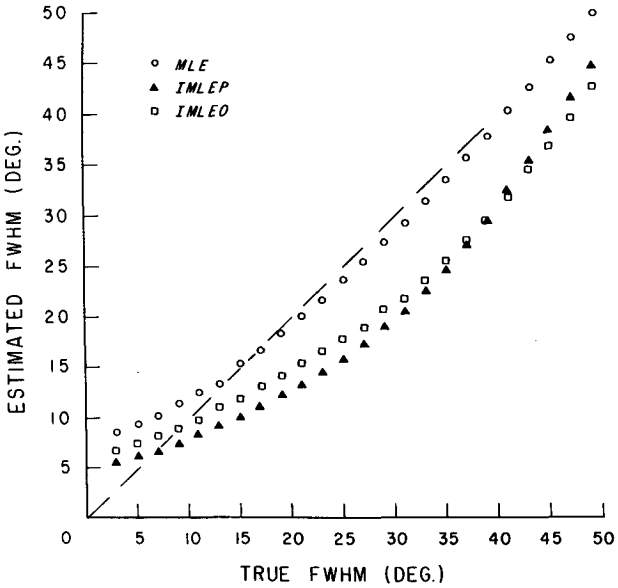

FIG. 3. Estimated versus true full width at half-maximum power (FWHM) for unimodal spectra, NSR = 0.05.

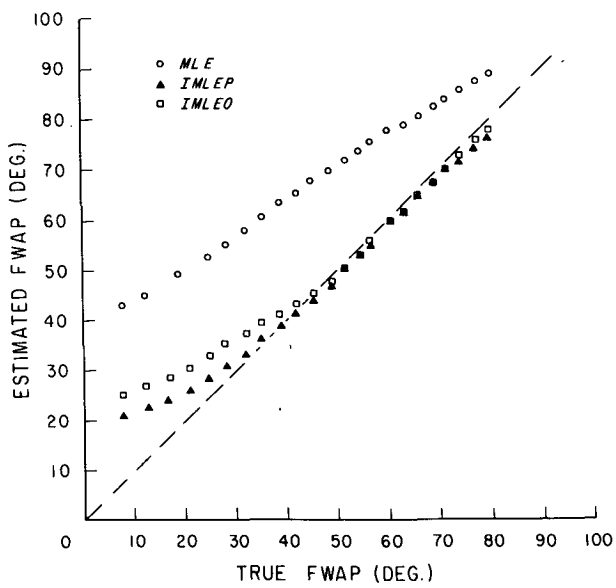

FIG. 4. Estimated versus true full width at average power (FWAP) for unimodal spectra, NSR = 0.05.

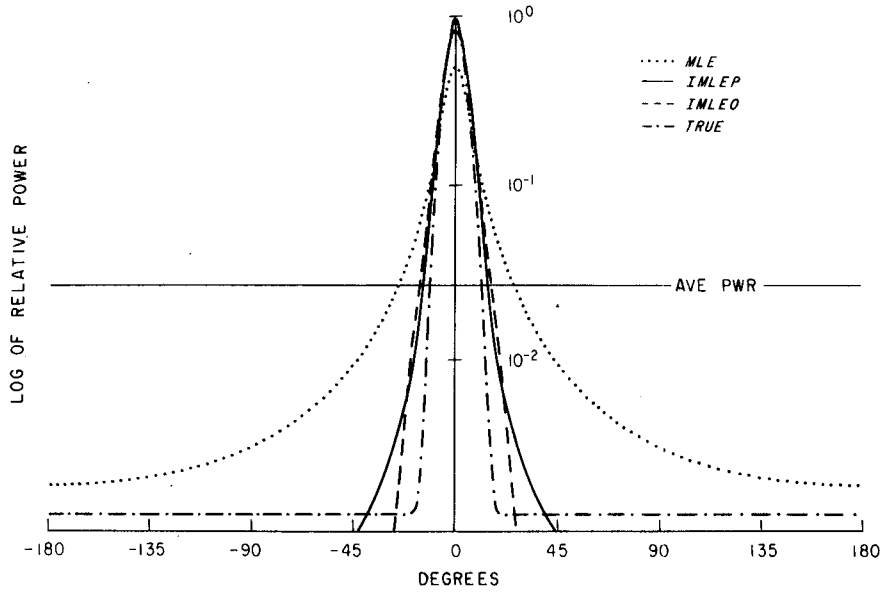

FIG. 5. A unimodal test spectrum with 10 degrees full width at half-maximum power (NSR = 0.05) and the MLE, IMLEP and IMLEO estimated spectra.

The superiority of the IMLE is more evident when estimating a bimodal spectrum. Figure 7 plots the WAPE values of the three estimators against the true-spectrum FWHM values. Both modes have the same shape and magnitude and are separated by 90 degrees.

A final look at estimator performance with deterministic data addresses the resolvability of directional modes. Figures 8 and 9 plot the estimated peak angles of each mode against angular separation of two modes with 10-degree FWHM. The modes are located at plus and minus one-half the angular separation. In Fig. 8 the two modes are of equal magnitude. The IMLEP, IMLEO and MLE were able to resolve

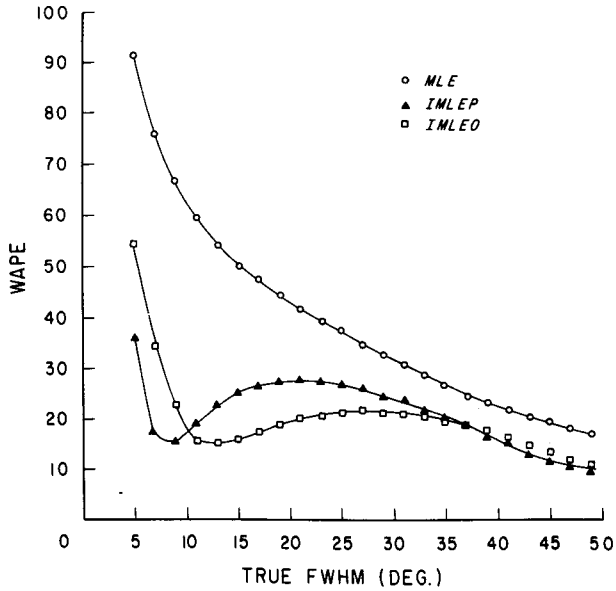

FIG. 6. The weighted average percent error (WAPE) fidelity of the three spectrum estimates of unimodal true spectra of varying full width at half-maximum power (FWHM), NSR = 0.05.

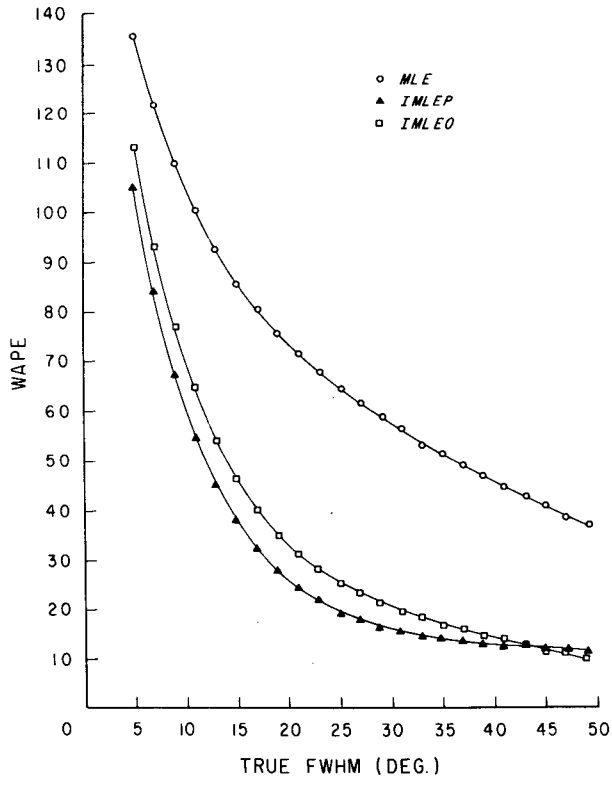

FIG. 7. The weighted average percent error (WAPE) fidelity of the three spectrum estimates of bimodal true spectra of varying full width at half-maximum power (FWHM), NSR = 0.05.

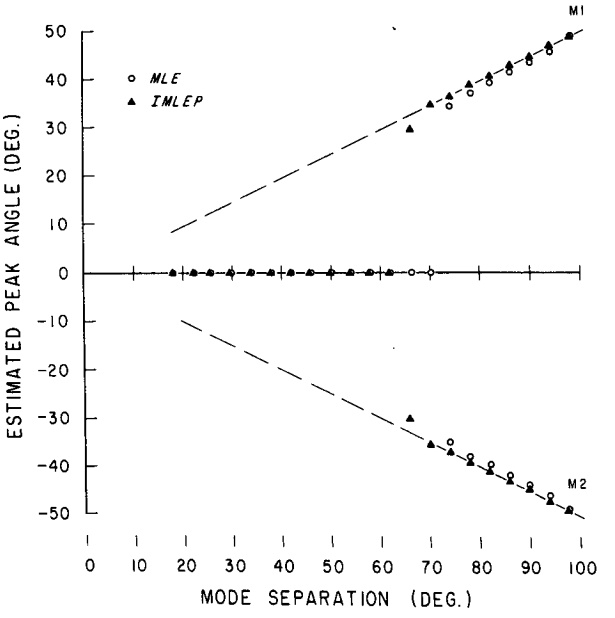

FIG. 8. Estimated peak angles of bimodal test spectra with varying angular separation of the modes. The modes (M1 and M2) have equal energy and are 10 degrees full width at half-maximum power, NSR = 0.05.

(defined as a spectral valley between peaks having less than half the power of the small peak) the modes at angle separations greater than 64 degrees, 68 degrees and 72 degrees respectively. When the modes were resolved, each mode's peak angle was well estimated. When the modes were not resolved, the peak power occurred midway between the true peaks (i.e., at 0°). The estimators' behavior for two modes of unequal magnitude is shown in Fig. 9. Mode 1 has one-half the peak power of mode 2. When the modes are not resolved, the estimated peak angle is shifted towards the larger mode (mode 2).

The performance of the two truncated Fourier-series estimators in this series of tests was very poor. For a unimodal spectrum with a true FWHM of 3 degrees, the weighted window and unweighted Fourier estimators had an estimated FWHM of 131 and 88 degrees respectively (compare to Fig. 3). The WAPE values for the two estimators were 237 and 180, respectively. These two estimators were unable to resolve the two modes in the bimodal spectra of Figs. 8 and 9.

Nondeterministic synthetic data were generated to examine the stability of the three spectrum estimators. Statistical fluctuations in the cross-spectral matrix were introduced following the method of Brennan and Mallet (1976). Their technique develops a vector of three complex Gaussian random numbers with zero mean and second moments defined by the deterministic cross-spectral matrix; the Gaussian vector is one synthetic realization of the Fourier coefficients of $\eta(t)$, $\eta_x(t)$ and $\eta_y(t)$.

Fifty statistically independent nondeterministic cross-spectral matrices were generated. Each matrix had roughly 30 degrees of freedom. The cross-spectral matrices were used to generate 50 spectrum estimates, each one being a statistical realization with 30 degrees of freedom of the true unimodal spectrum (peak angle = 0°, FWHM = 10°). The average peak angle of the 50 MLE estimates was 0.12 degrees, with a standard deviation of 1.32 degrees. The IMLE statistics were similar. These estimators do not exhibit any stability problems.

4. Field data

Slope array data were collected during February 1980 as part of the Nearshore Sediment Transport Study at Leadbetter Beach, California (Gable, 1981). The slope array was located in about 9 m depth, offshore of about 20 electromagnetic current meters deployed in the surf area. One major purpose of the slope array was to provide directional information about the incident wave field driving longshore currents within the surf zone. The emphasis here is on demonstrating that the new data-adaptive estimators yield physically realistic directional spectra in a field application.

The Leadbetter Beach site is well suited for this purpose because there are only two narrow apertures through which long gravity waves can pass (Fig. 10). The fetch between Santa Barbara and the Channel

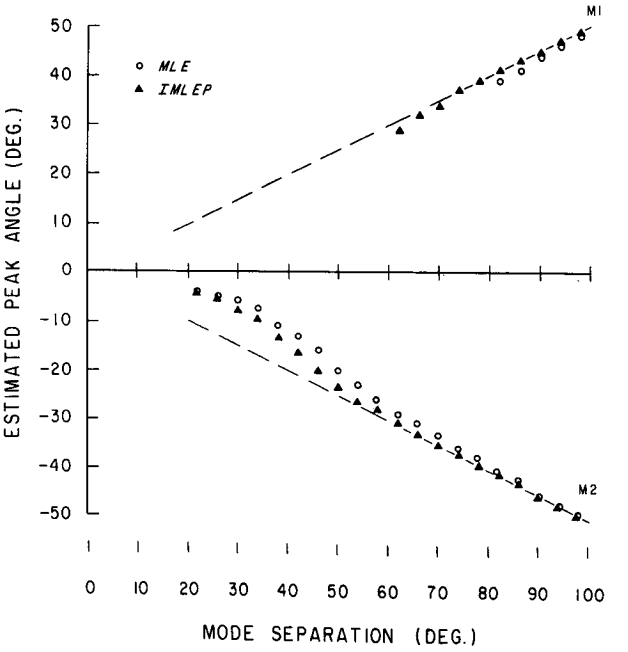

FIG. 9. Estimated peak angles of bimodal test spectra with varying angular separation of the modes. One mode (M1) has half the energy of the other (M2). Both modes are 10 degrees full width at half-maximum power, NSR = 0.05.

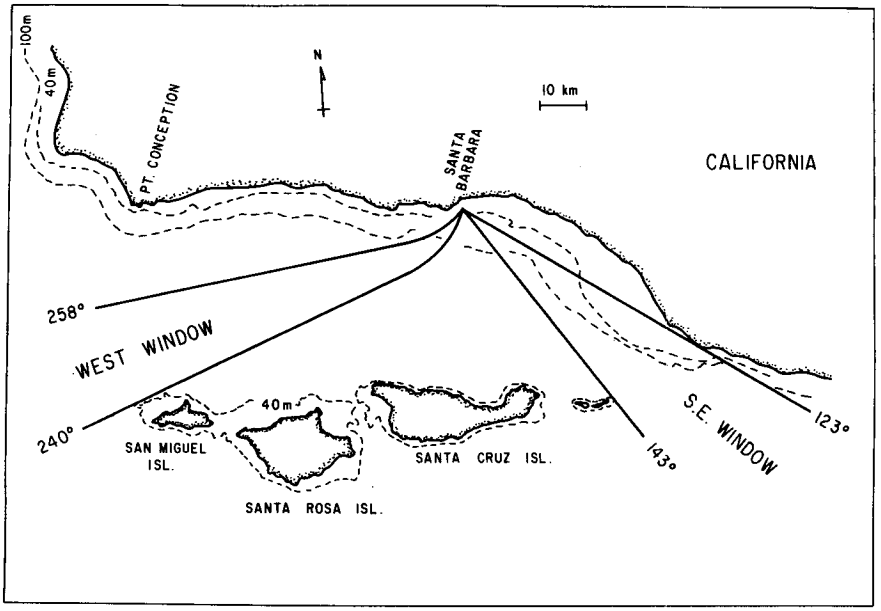

FIG. 10. Bathymetry in the region of Santa Barbara, California.

Islands is too short (50 km) for local generation of long gravity waves.

Refraction calculations determined the possible angular range of waves incident on the slope array from the west window (240–258° on Fig. 10). For a frequency of 0.075 Hz, only a small angular range of incident wave angles (at the array) was observed to map back into the deep ocean. Angles greater than 188 degrees could not escape the coastal bathymetry, while angles less than 184 degrees hit the Channel Islands. The southeast window (123–143° on Fig. 10) has a restricted fetch (150 km) and is not generally energetic, although substantial energy did occasionally come from this quadrant during the experiment. If rays with these angles were effected only by the topography directly offshore of the array, and that topography was plane and parallel to Leadbetter Beach, then Snell's law maps the deep ocean angles to 124–144 degrees (for f = 0.25 Hz) at the array. The salient point is that most frequencies can only reach the slope array from two narrow sources which are separated by about 100 degrees in deep water. Typically, low-frequency energy is expected out of the west window and high-frequency energy is expected out of either window dependent upon local wind conditions.

The cross-spectral data matrix [Eq. (1)] needed for calculation of the directional spectra was obtained from the four bottom-mounted pressure sensors of the slope array. The time series of each pressure sensor was Fourier transformed. Linear theory was used to calculate the Fourier coefficients of sea surface elevation from the pressure coefficients. An inverse Fourier transform produced time series of sea surface elevation above each pressure sensor. At each time sample, a two-dimensional plane surface was fit to the sea surface elevations yielding time series of sea surface elevation (η) and slopes (η_x, η_y). Only three sensors are required for this procedure; the fourth sensor reduces noise-related errors. Fourier transforms of η, η_x and η_y produce the coefficients required in Eq. (1). The spectra discussed below are calculated from 2 hours of data. Averaging resulted in a frequency bandwidth of 0.0078 Hz and 112 degrees of freedom.

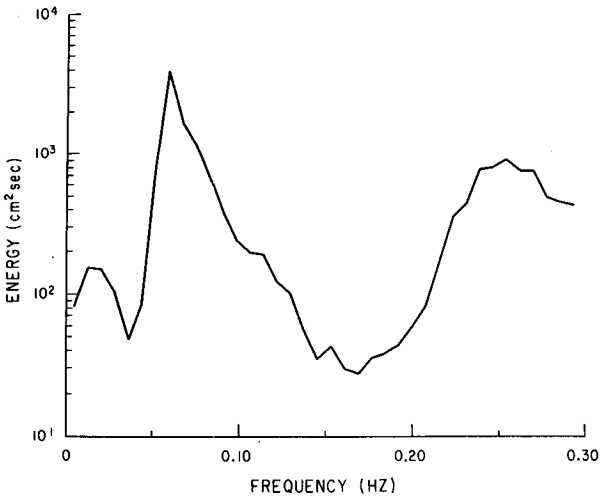

FIG. 11. Energy spectrum for 12 February (112 degrees of freedom, Δf = 0.0078 Hz).

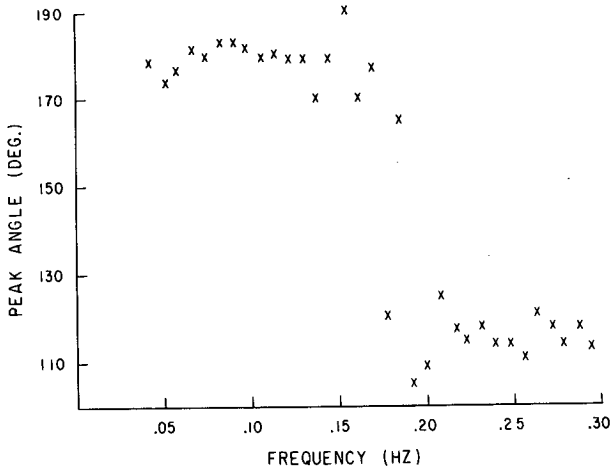

FIG. 12. Peak mode angle versus frequency for 12 February.

On several days of the experiment, local winds blowing from the southeast created a mixed sea with both swell and wind chop peaks in the energy spectrum (Fig. 11)]. An example of the estimated (IMLEP) angle of maximum power at the slope array under these conditions is shown in Fig. 12. The variation of the mode peak angle with frequency clearly shows low-frequency waves ($f < 0.13$ Hz) from the west and high frequency waves ($f > 0.19$ Hz) predominantly from the east. At intermediate frequencies ($0.13 < f < 0.19$ Hz) the spectrum would be expected to be bimodal, providing a field test of the estimators' ability to resolve two directional modes. At the two peaks of the energy spectrum ($f = 0.059$ and 0.250 Hz on Fig. 11), the observed directional spectra are relatively narrow and have peak energy at angles corresponding to the west and east windows respectively (Fig. 13). At an intermediate frequency, 0.153 Hz, two peaks are present in the estimated spectrum. However, a nearby frequency ($f = 0.138$ Hz) shows a unimodal structure centered between the expected peaks.

The spectrum estimators behave in a realistic manner with these field data. They show the expected incident-wave direction transition with frequency and are marginally able to resolve the two directional modes at the intermediate frequencies. The marginal resolution is not unexpected. The deterministic synthetic-data resolution analysis (Figs. 8 and 9) indicates that the angular separation of these two modes (approximately 70°) barely allows resolution.

5. Summary

Maximum likelihood (MLE) and iterative MLE (IMLE) directional estimators, similar to those successfully used with spatial arrays (Davis and Regier, 1977; Pawka, 1982, 1983), have been developed for "point" measurement systems. These estimators do not require *a priori* assumptions about the true shape of the directional spectrum. Improved resolution is obtained with data-adaptive assumptions about the true spectrum. These estimators have numerical algorithms that are relatively simple and computationally fast.

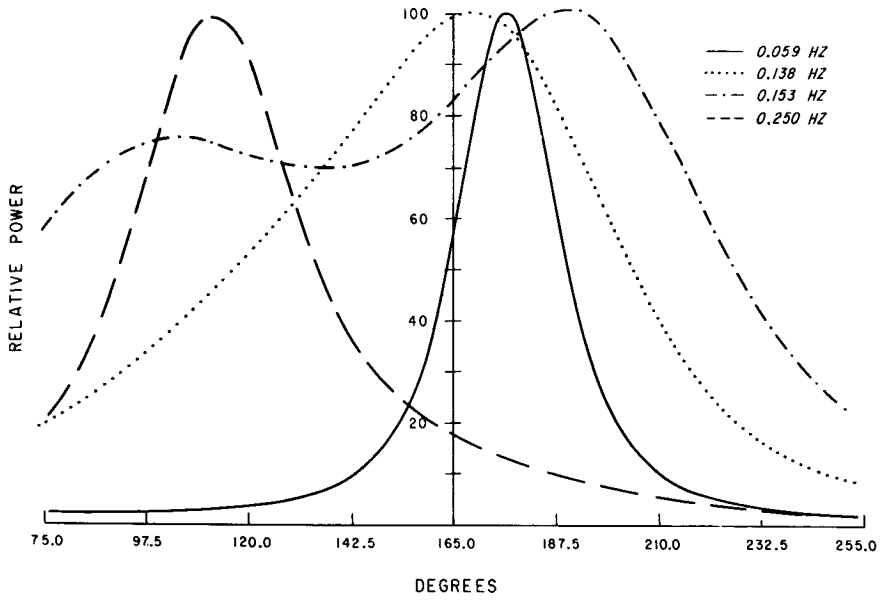

FIG. 13. IMLEP directional spectra (112 degrees of freedom) for four frequencies on 12 February. Each spectrum is scaled to have maximum density 100.

The IMLE is an iterative algorithm that operates on the MLE spectrum. It has better resolution than the MLE and, unlike the MLE, is a possible true spectrum. The IMLE iterative algorithm develops a spectrum that can be used to reconstruct the original cross-spectral data matrix. Two variations of the IMLE iterative correction term [Eqs. (8) and (9)] have been used and found to yield very similar estimated spectra.

The performance of these estimators with deterministic data was good (Figs. 1–9) and found to be similar for either Gaussian or cosine power mode shapes. In fact a wide range of smooth shapes can be similarly well estimated; this is a distinct advantage over the cosine power parameterization of Lonquet-Higgins *et al.* (1963).

The peak angle of unimodal test spectra was always correctly estimated. Mode-shape parameters such as full width at half maximum (FWHM) were reasonably well estimated (Figs. 3 and 4). However, the IMLE at times overresolved peaks, underestimating the FWHM.

A significant improvement in directional-spectrum estimation provided by these data-adaptive estimators is the ability to resolve some bimodal spectra. The unweighted truncated Fourier-series estimation method was only able to resolve modes separated by greater than 120 degrees and the unimodal cosine-power parameterization by definition should not be used with possible bimodal spectra. These data adaptive estimators were able to resolve spectral modes with 10 degrees FWHM at approximately 70 degrees separation for deterministic synthetic data (Figs. 8 and 9). The synthetic data further showed that if two modes are of equal energy and not resolvable, the estimated peak angle will fall symmetrically between the peak angles of the two modes. If they are of unequal energy, the estimated peak angle will be skewed towards the more energetic mode. Field data at Santa Barbara, California indicated similar behavior.

These spectrum estimators appear to be stable and give reasonable estimates with nondeterministic data. Nondeterministic synthetic data were generated from a true, unimodal spectrum with peak angle at 0 degrees and a FWHM of 10 degrees. The average estimated peak angle from 50 statistical realizations of the true spectrum was 0.12 degrees, with a standard deviation of 1.32 degrees. The field data at Santa Barbara, California were found to yield physically realistic directional spectra from cross-spectral matrices with 112 degrees of freedom.

Acknowledgments. This research was supported by NSF grant OCE-8213657. S. S. Pawka suggested application of MLE techniques to point array measurements, and made many valuable and insightful suggestions. Joan Semler typed the manuscript and Michael Clark drafted the figures.

REFERENCES

Borgman, L. E., and E. Yfantis, 1979: Three-dimensional character of waves and forces. *ASCE Civil Engineering in the Oceans,* Vol. 4, 791–804.

Bowden, K. F., and R. A. White, 1966: Measurements of the orbital velocities of sea waves and their use in determining the directional spectrum. *Geophys. J. Roy. Astron. Soc.,* **12,** 33–54.

Brennan, L. E., and J. D. Mallet, 1976: Efficient simulation of external noise incident on arrays. *IEEE Trans. on Antennas and Propagation,* **24,** 740–741.

Burg, J. P., 1972: The relationship between maximum entropy spectra and maximum likelihood spectra. *Geophysics,* **37,** 375–376.

Capon, J., R. J. Greenfield and R. J. Kolker, 1967: Multidimensional maximum-likelihood processing of a large aperture seismic array. *Proc. IEEE,* **55,** 192–211.

Cartwright, D. E., 1963: The use of directional spectra in studying the output of a wave recorder on a movstudying ship. *Proc. Conf. Ocean Wave Spectra,* Easton, MD, Prentice-Hall, 203–218.

——, and N. D. Smith, 1964: Buoy techniques for obtaining directional wave spectra. *Buoy Technology,* Washington, DC, Mar. Technol. Soc., 112–121.

Davis, R. E., and L. A. Regier, 1977: Methods for estimating directional wave spectra from multi-element arrays. *J. Mar. Res.,* **35,** 453–477.

Forristall, G. Z., E. G. Ward, V. J. Cardone and L. E. Borgmann, 1978: The directional spectra and kinematics of surface gravity waves in tropical storm Delia. *J. Phys. Oceanogr.,* **8,** 888–909.

Gable, C. G., Ed., 1981: Report on data from the Nearshore Sediment Transport Study Experiment at Leadbetter Beach, Santa Barbara, California, January–February 1980. IMR Ref. No. 80-5, University of California, Inst. Mar. Resour., La Jolla, CA.

Higgins, A. L., R. J. Seymour and S. S. Pawka, 1981: A compact representation of ocean wave directionality. *Appl. Ocean Res.,* **3,** 105–112.

Long, R. B., and K. Hasselmann, 1979: A variational technique for extracting directional spectra from multi-component wave data. *J. Phys. Oceanogr.,* **9,** 373–381.

Longuet-Higgins, M. S., D. E. Cartwright and N. D. Smith, 1963: Observations of the directional spectrum of sea waves using the motions of a floating buoy. *Proc. Conf. Ocean Wave Spectra,* Prentice-Hall, 111–132.

Mitsuyasu, H., F. Tasai, T. Suhara, S. Mizuno, M. Ohkuso, T. Honda and K. Rikishi, 1975: Observations of the directional spectrum of ocean waves using a cloverleaf buoy. *J. Phys. Oceanogr.,* **5,** 750–758.

Nagata, Y., 1964: The statistical properties of orbital wave motions and their application for the measurement of directional wave spectra. *J. Oceanogr. Soc. Japan,* **19,** 169–181.

Pawka, S. S., 1982: Wave directional characteristics on a partially sheltered coast. Ph.D. dissertation, University of California, San Diego, 246 pp.

——, 1983: Island shadows in wave directional spectra. *J. Geophys. Res.,* **88,** 2579–2591.

——, D. L. Inman and R. T. Guza, 1984a: Island sheltering of surface gravity waves: model and experiment. *Continental Shelf Res.,* **3**(1), 35–53.

——, —— and ——, 1984b: Radiation stress estimators. *J. Phys. Oceanogr.,* **13,** 1698–1708.

Regier, L. A., and R. E. Davis, 1977: Observations of the power and directional spectrum of ocean surface waves. *J. Mar. Res.,* **35,** 433–452.

Seymour, R. J., and A. L. Higgins, 1977: A slope array for measuring wave direction. *Proc. Workshop on Coastal Processes Instrumentation.* La Jolla, University of California, San Diego, Sea Grant Publ. No. 62, IMR Ref. No. 78-102, 133–142.

Simpson, J. H., 1969: Observations of the directional characteristics of sea waves. *Geophys. J. Roy. Astron. Soc.,* **17,** 93–120.